

Experimental and numerical mechanical characterisation of additively manufactured polymeric lattice structures under uniaxial tensile load

Original

Experimental and numerical mechanical characterisation of additively manufactured polymeric lattice structures under uniaxial tensile load / Bruson, D.; Iuliano, L.; Galati, M.. - In: MECCANICA. - ISSN 0025-6455. - (2024).
[10.1007/s11012-024-01813-2]

Availability:

This version is available at: 11583/2992283 since: 2024-09-06T12:41:07Z

Publisher:

Springer Science and Business Media B.V.

Published

DOI:10.1007/s11012-024-01813-2

Terms of use:

This article is made available under terms and conditions as specified in the corresponding bibliographic description in the repository

Publisher copyright

(Article begins on next page)



Experimental and numerical mechanical characterisation of additively manufactured polymeric lattice structures under uniaxial tensile load

Danilo Bruson · Luca Iuliano · Manuela Galati

Received: 23 November 2023 / Accepted: 22 April 2024
© The Author(s) 2024

Abstract Additive manufacturing enables the production of lighter, more robust components with intricate features like lattice structures. However, since the mechanical behaviour of lattice structures is not fully characterized, the application of such potential is limited today. The challenge with lattice structures tensile tests is defining a suitable design that fits the standard requirements and process characteristics. In the polymeric powder bed fusion process, the problem is to produce powder-free geometries and to avoid stress concentrations zones, adapting the specimen accordingly. In this regard, numerical simulation may provide insightful information and support the analysis of the deformation mechanisms. This paper analyses a new tensile sample for lattice structures using finite element analysis. The sample is designed following the EN ISO 527 standard prescriptions. An area with a controlled gradation of the lattice relative density is designed to ensure both powder-free voids and fracture localization within the lattice specimen gauge length. Experimental tests are performed to validate the numerical results using a modified body cubic centred topology with two different strut diameters. The specimens are produced in polyamide by powder bed AM process. Due to the complexity of the lattice design, a digital image correlation is used

to compute the full range of strains at the macroscopic level. Experimental and numerical strain maps results showed a good agreement. The recorded deviation was attributed to the process-induced defect, such as the geometrical accuracy that, if compensated, boosted the capability of the numerical model to predict the mechanical behaviour of the lattice structure.

Keywords Lattice structures · Tensile · FEA · PBF-LB/P · Nylon · Selective laser sintering

1 Introduction

Reticular structures, also called lattices, are geometrical features that describe the absence of design constraints in advanced technologies such as additive manufacturing (AM). Despite this possibility, the use of such structures is still limited because little information is present on their mechanical behaviour and feature quality.

Because of the reticular nature of the lattice structures, the main issue from the manufacturing point of view is to guarantee adequate dimensional accuracy with respect to the nominally designed structures [1–4].

From the mechanical point of view, lattice structures have been primarily investigated under compression loads [5–14], while few works have been focused on the tensile behaviour [15, 16]. The main problem when testing lattice structures under tensile

D. Bruson (✉) · L. Iuliano · M. Galati
Department of Management and Production Engineering,
Politecnico di Torino, Turin, Italy
e-mail: danilo.bruson@polito.it

load is the discontinuities in the stress distribution located in the load introduction zone [15, 17, 18]. This discontinuity provokes a fracture outside the gauge length or at the boundary between the lattice and the bulk end [17], invalidating the result. To solve this issue, Drücker et al. [15] proved that a smooth transition at that boundary could distribute the stress during the loading more uniformly. Practically, this proposal was realised by progressively increasing the strut diameter to obtain a gradual density gradation that enables control of the fracture localisation. Despite the potential of this approach, only a few examples can be found in literature, and they are mainly devoted to metallic materials [19, 20]. For polymeric materials, the tensile behaviour of stochastic Voronoi and a body-centred cubic structure has been investigated by Porter et al. [21] using experiments and finite element (FE) method. The samples were designed without any gradation. The deviation between the experimental and numerical force–displacement was over 97%. Overall, this large deviation observed in literature was explained by numerous works as the effect of manufacturing errors and dimensional deviations, which are usually not considered by the numerical models [5, 22]. It has been demonstrated that the deviation between the CAD model and the actual fabrication is significant, especially in the case of thin structures [22].

Besides manufacturing, another challenge for the mechanical characterisation of such thin and complex structures is acquiring the full range of local strain distribution under load. Using an extensometer that gives the average strain is meaningless for such structures. The use of a digital image correlation (DIC) system may provide a deeper understanding of local deformations [23–25]. However, the acquired images need to be processed meticulously because of the pattern created by projecting the structures in 2 dimensions. Also, the outcomes of DIC analysis in such reticular structures may be affected by acquisition factors, including magnification, lens quality, light conditions, and the complexity of the surface texture of the specimen [24]. Extended strut topologies can exhibit significant out-of-plane displacements when performing DIC analysis on lattice structures [24]. Inclined struts relative to the 2D image acquisition plane could present a strain accumulation phenomenon on the

out-of-plane strain tensor components, leading to an underestimation of their actual deformation [25].

Another challenging point of applying the density gradation approach is modelling the density gradation because it should simultaneously consider the gradation pattern, its extension, the variation of density and the manufacturing constraints. Because the playing variables are multiples, predicting the fracture is difficult. The simulation could help to forecast the fracture localisation and analyse the stress/strain distribution in advance. This data could then be used to adjust the specimen geometry and prevent stress concentration outside the gauge length.

Considering the literature, this work attempts to implement a non-linear FE model with improved predictive capabilities and analyse the effect of density gradation of the lattice cell on the load introduction and corresponding stress. As a novelty, the geometry proposed for the numerical and experimental lattice specimen adapts to the ISO 527 standard for plastics. In addition, a new formulation was used to obtain the density gradation. The samples were fabricated using polyamide PA12 and a laser powder bed fusion system and then tested under a quasi-static tensile test. DIC measurements were performed during the test to assess further the designed geometry efficacy and validate the simulation model. The influence of the process-induced defects on the numerical results was investigated via X-ray computed tomography.

2 Material and methods

The EN ISO 527-2:2019 [26] standard tensile sample for plastics (Fig. 1) was selected as a standard for creating the geometry.

The selected cell for the analysis was the body cubic centred (BCC) topology due to the wide literature research on this type of structure [8, 11, 14, 21, 27–30]. It consists of 4 diagonal struts oriented as the diagonals of a cube and merged in a single central node. In the analysed configuration, displayed in Fig. 2b), the classic form of BCC has been inscribed in a cubic primitive cell made of struts placed along the edges of a cube to improve the bending stiffness of the tensile specimen.

The fitting of the lattice structure in the standard geometry involved replacing the gauge length with the unit cells at a predefined relative density. From the

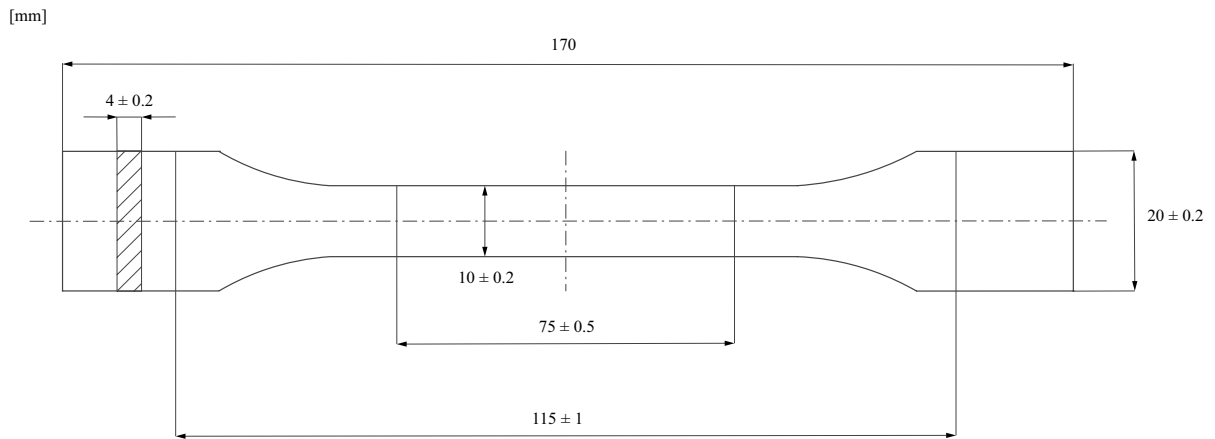


Fig. 1 EN ISO 527-2:2019: specimen type 1A [26]. Dimension in mm

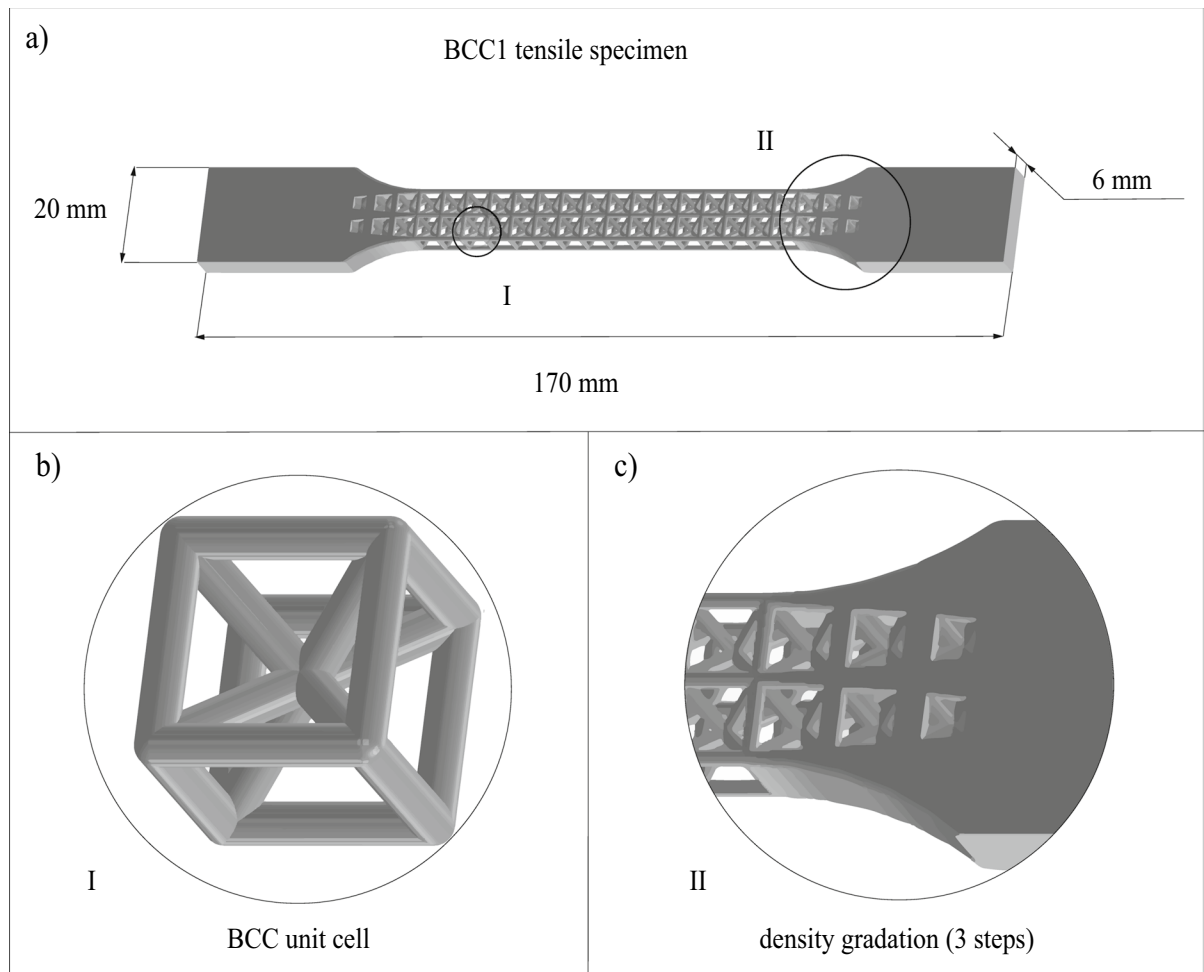


Fig. 2 Specimen dimensioning with the detailed view of the BCC1 unit cell topology and the three density gradation steps at the lattice-bulk interface

end of the gauge length, a smooth transition is realised by gradually increasing each strut diameter. The cell dimension has been selected for the experimental validation, in compliance with the standard, equal to 5 mm. The elementary cell was investigated using two different strut diameters. The first structure, BCC1, has struts with a corresponding diameter equal to 1 mm and a relative density in the gauge length equal to 25%. The second structure was named BCC1.5 and had struts with a diameter equal to 1.5 mm and a corresponding relative density in the gauge length equal to 45%. For both cases, the width-thickness ratio was kept constant and equal to approximately 10:4.

The specimen thickness has been designed to include only one elementary cell. Therefore, the width and thickness of the standard specimen were slightly adjusted to 11 and 6 mm, respectively, for BCC1 and 11.5 mm and 6.5 mm for BCC1.5.

Unlike the approach that Drücker et al. adopted [15], the gradation was designed to achieve a complete fusion between the lattice and the bulk ends. That means that the diameter of the strut at the last step of gradation corresponds to a relative density of at least 90% of the bulk density. This gradation has been achieved in three steps. At each step, the diameter has been increased with respect to the previous step (Fig. 2) by 44% for BCC1 and 26% for BCC1.5. In this way, a gradual decrease of the void volume of the cell was realised, accomplishing a smooth transition from the lattice to the bulk ends.

Parallel to the design for the production, a finite element analysis has been performed on the preliminary design using ANSYS Workbench 2021 (ANSYS Inc.; Canonsburg, PA). The analysis aims to assess the efficacy of the adopted gradation pattern to guarantee the homogeneity of the stress distribution within the gauge length of the sample. The model has been discretised with second-order 10-node quadratic tetrahedron SOLID 187 elements with a size equal to 0.20 mm, selected after a convergence analysis and, accordingly, the strut size. Considering the geometry and material-related non-linearities, a “Static Structural” analysis via Newton–Raphson Method as non-linear solution strategy was adopted with “Large deflections” and

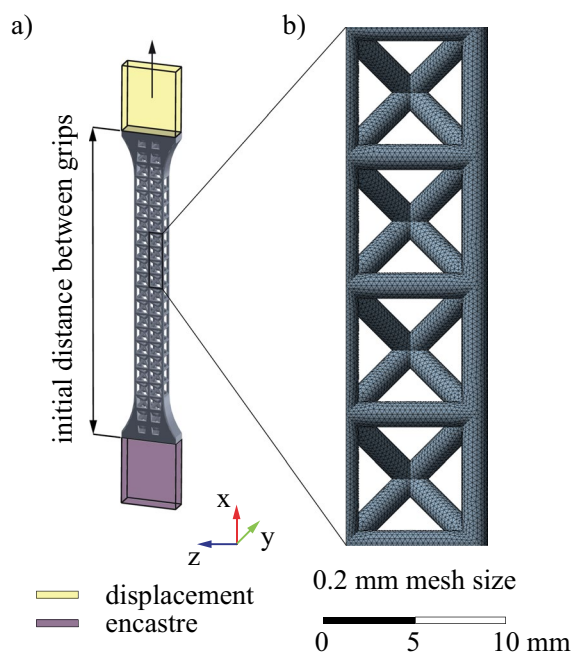


Fig. 3 **a** Model used to simulate the BCC1 tensile test, **b** Segment of the BCC1 lattice specimen meshed cells with a 0.2 mm mesh size

“Quasi-static solution” options activated in the solver controls panel.

According to Porter et al. [21], the material used in the analysis was modelled using a multi-linear isotropic hardening (MISO) material. This model accounts for the linear-elastic and plasticity of the material. The Young’s Modulus of 1345 MPa and the plasticity piece-wise vector reported in Table 1 have been derived from the tensile tests performed on bulk specimens built in the same conditions used for the lattice samples. The Poisson ratio was set at 0.4 accordingly Ref. [5, 21, 31].

The analysis was performed by applying a joint constraint to the two surfaces of one end tab to replicate the clamp, while a longitudinal displacement of 3 mm was applied to the opposite tab. For example, Fig. 3a illustrates the model for the BCC1 structures with a portion of the lattice specimen with the detail of the discretisation (Fig. 3b).

Table 1 True plastic stress and strain of bulk material

Yield stress (Mpa)	21.2	24.5	27.7	30.8	36.2	43	47.8	49.3
Plastic strain	0.0000	0.0003	0.0006	0.0010	0.0024	0.0800	0.0180	0.0300

The specimens were fabricated using PA2200 powder (polyamide 12 or PA12, with a mixture of 50% virgin and 50% recycled) and an EOS Formiga P110 Velocis system laser, a powder bed fusion (PBF-LB) system. The process parameters were set as in Ref. [32]. The samples were built in the edgewise configuration, thus with the sample thickness perpendicular to the build orientation (z-axis), as shown in Fig. 4a).

Five replicas were produced for each geometry (BCC1 and BCC15). In addition, as anticipated before, five bulk samples were also manufactured to extract and model the numerical material model.

All the tensile tests were carried out using an Easydur AURA 10 T system following EN ISO 527-1 [33]. The crosshead speed was equal to 5 mm/min, and the acquisition rate was at 500 Hz until the sample failed. The replicas were used to validate the replicability of the process. Figure 5 shows the results of tensile tests in terms of force–displacement for the replicas of each analysed structures. As

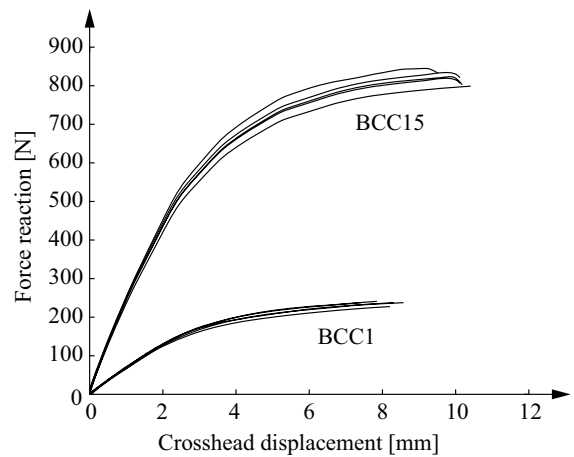


Fig. 5 Experimental BCC15 and BCC1 force–displacement plot

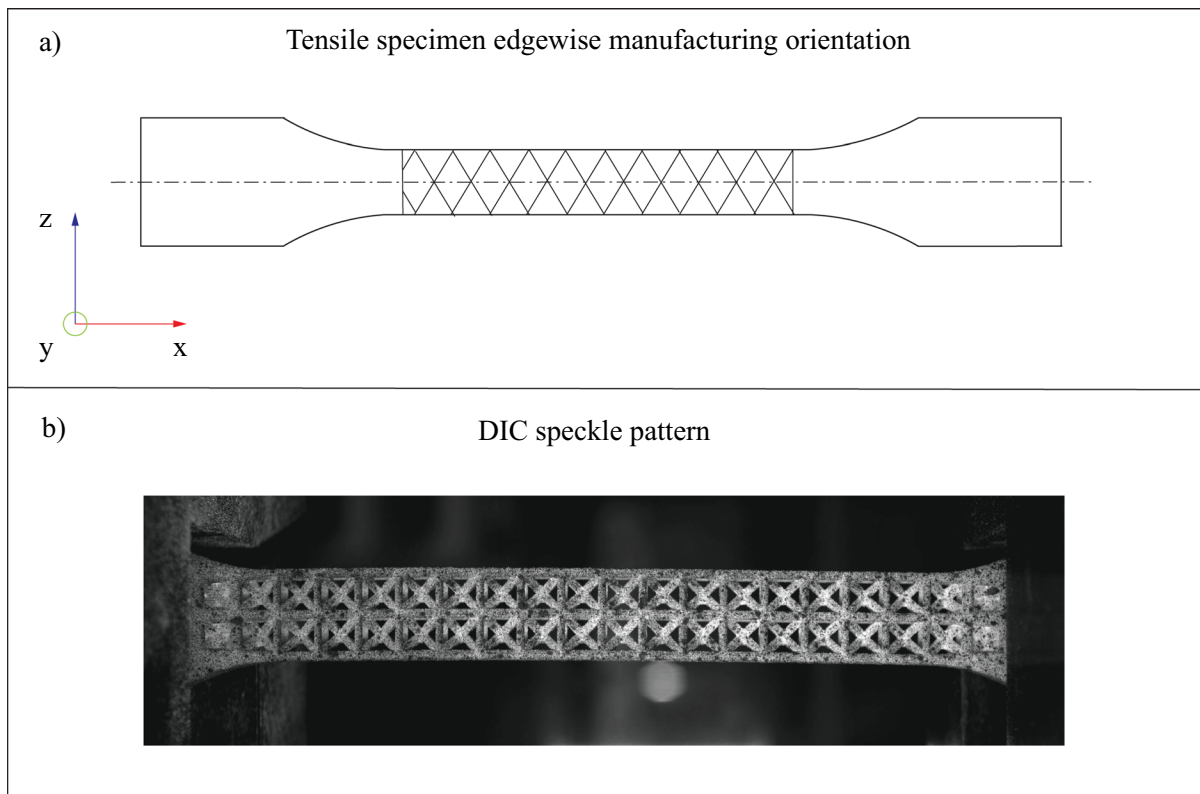


Fig. 4 **a** Manufacturing edgewise orientation of the tensile specimen (z build orientation) and **b** BCC1 DIC speckle pattern

it can be observed, the deviation among the different tests is negligible considering the scope of the paper.

Before the test, the lattice specimens were coated with white aerosol paint and a speckled pattern via black aerosol paint, as reported in Fig. 4b). The pattern highlights the local deformation of the sample for an automatic DIC. The images for the DIC were acquired at 1 fps with an X-Sight optical extensometer and then processed via the open-source Matlab code Ncorr.

The dimensional and porosity analyses of the manufactured specimens were carried out using a computed tomography (CT-scan) system, GE Phoenix vltomelx s. The tomographies were acquired using 100 kV of voltage, 80 μ A of current, and a

corresponding voxel size of 16.74 μ m. The 3D geometry was modelled using the software VGStudio Max 3.4.

3 Results and discussion

The numerical results showed that the designed sample provides a homogeneous stress distribution in the load introduction region without any perturbations at the bulk-lattice interface. An example of the results is reported in Fig. 6 as Von Mises stress plots of the BCC1 and BCC1.5 (Fig. 5b). As can be observed, the regions of high stress (red zones) are located within the gauge length as recommended by the standard and the values decrease toward the bulk ends.

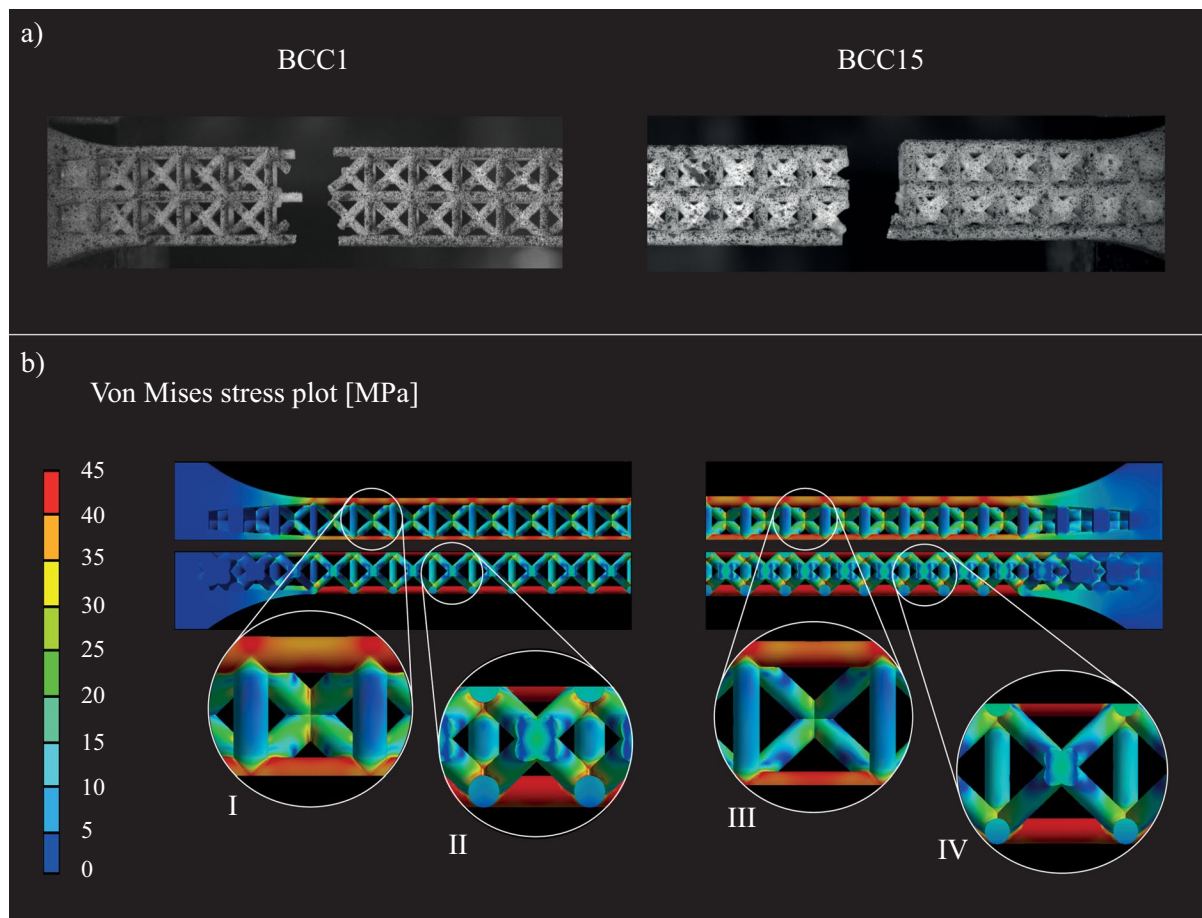


Fig. 6 **a** Failed specimens after the tensile tests compared to the **b** Von Mises stress plots at 3 mm of crosshead displacements. I–III front view of BCC1 and BCC1.5 single cell stress

plot magnifications, II–IV middle plane section view of BCC1 and BCC1.5 single cell stress plot magnifications

This result is confirmed by the experimental tests (Fig. 5a), in which all failures occurred within the gauge length of the lattice specimen on a single cell row level. This behaviour, therefore, validates the uniform load introduction.

As can be observed in the magnification in Fig. 6, the most stressed regions are detected along the longitudinal struts oriented along the tensile load axis. In particular, the higher stress areas are located internally on longitudinal struts, as shown in the mid-plane section stress plots. The beams arranged along the diagonal and perpendicular displayed stress values mostly lower than half of the maximum stress magnitude.

The stresses are located in the nodal regions of the longitudinal beams, indicating likely a failure location at the single-cell level, according to the experimental results (Fig. 6b).

The load-bearing capacity of the analysed topology is mainly due to the longitudinal and diagonal struts. The higher stress located at the nodes can be

explained by the sharp re-entrant corners [21]. This effect appears more critical for the strut diameter equal to 1.5 mm where the stress at the central node was higher.

Good agreement has been found between the estimated location of higher stress and the position where the fracture occurred during the experiments. As mentioned above, the fractures occurred in the longitudinal struts of the specimen (Fig. 6a), which validates the numerical model.

To gain further insight into the pattern deformation of the analysed topology, Fig. 7 compares DIC measurements and the numerical simulations at a displacement of 2 mm. A good agreement can be observed regarding the strain distribution between the measured deformation through DIC and FE results, particularly for the predicted strains exhibited in the longitudinal and perpendicular struts relative to the tensile axis. The DIC strain plots showed good agreement with the numerical simulation results. This result confirms the homogeneous distribution of the

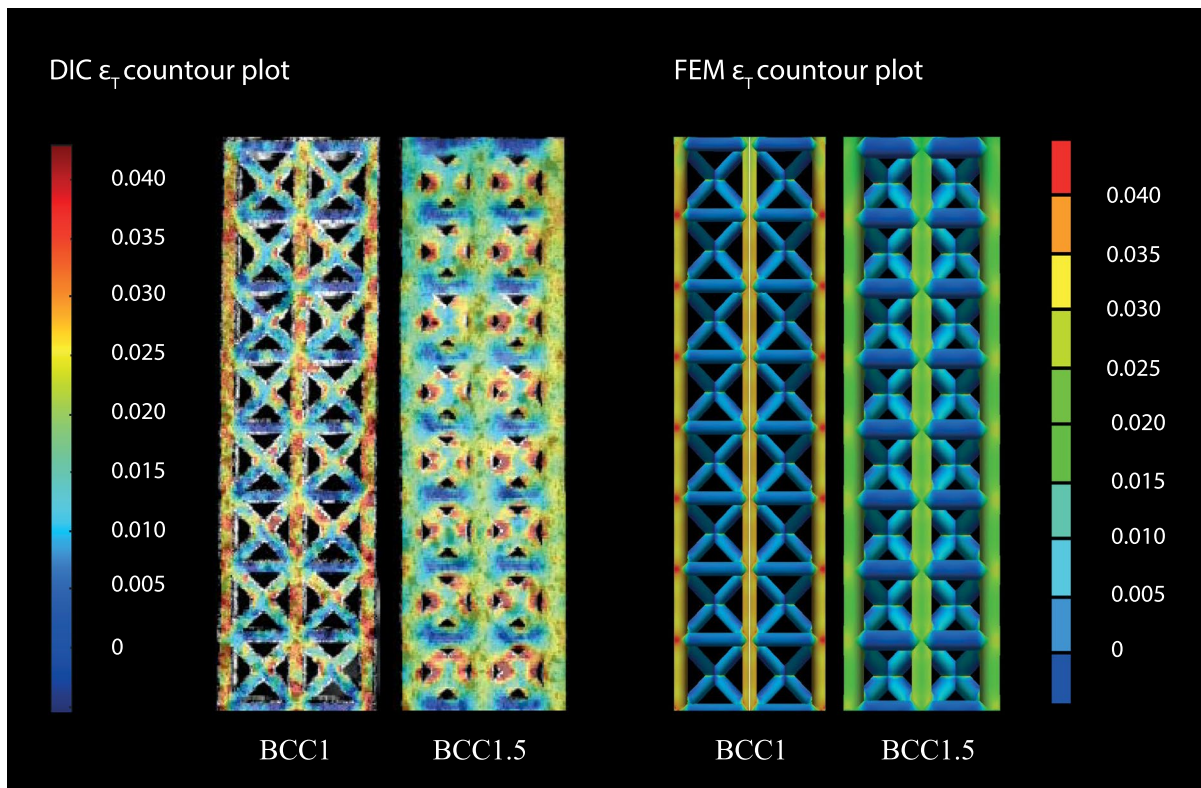


Fig. 7 DIC and FEA longitudinal strain ϵ_T contour plots of the BCC1 and BCC1.5 lattice specimens

cell strains along the gauge length and validates the efficacy of the designed load introduction geometry for the tensile testing of lattice structures. Numerically, the values differ for several reasons. Among them was the presence of process-induced geometrical defects on the strut surfaces that were neglected in the numerical model. The effect of the manufacturing system on the lattice caused strain concentrations that can be noticed in the diagonal struts. This phenomenon is more evident in the smaller strut size (1 mm), which agrees with previous results on the geometrical accuracy investigation of thin cylindrical elements [4].

For BCC1.5, the DIC analysis shows higher strains with respect to the corresponding numerical values, and they are located in the central node of the cell where the diagonal struts join. This behaviour could be observed in Fig. 6a) at a single cell level. BCC1 specimens tend instead to shift the strain localisations from the nodal area along the diagonal struts, resulting in a more homogeneous strain distribution.

To explain this behaviour, a further comparison is made between the forecasted force–displacement curves and the experimental values (Fig. 8). In this regard, the numerical model appeared stiffer than the experimental counterpart. At a crosshead displacement of 3 mm, the deviation between the calculated

and experimental force was around 47% and 7% for the BCC1 and BCC1.5, respectively. According to Ref. [5, 21, 22], the deviation could be attributed to geometrical or material differences between the experimental and numerical models. For the first issue, the geometry of the numerical model can be corrected by accurate dimensional analysis, such as CT-scan measurements. This analysis showed that the section of the horizontal struts is ovalised with respect to the circular CAD model. The measurements of the axes of the ellipse approximating the actual strut section for the horizontal strut are gathered in Table 2. Also, the struts that were oriented according to the build direction and the diagonal struts exhibited a

Table 2 BCC manufactured sample strut's measurements and standard deviations (SD)

Actual strut dimensions (SD)		BCC1	BCC1.5
(mm)			
x	Major axis a	1.08 (0.03)	1.55 (0.04)
	Minor axis b	0.60 (0.04)	1.28 (0.02)
y	Major axis a	1.13 (0.05)	1.58 (0.02)
	Minor axis b	0.64 (0.02)	1.31 (0.03)
z	Diameter	0.76 (0.04)	1.27 (0.05)
diag	Diameter	0.73 (0.02)	1.36 (0.03)

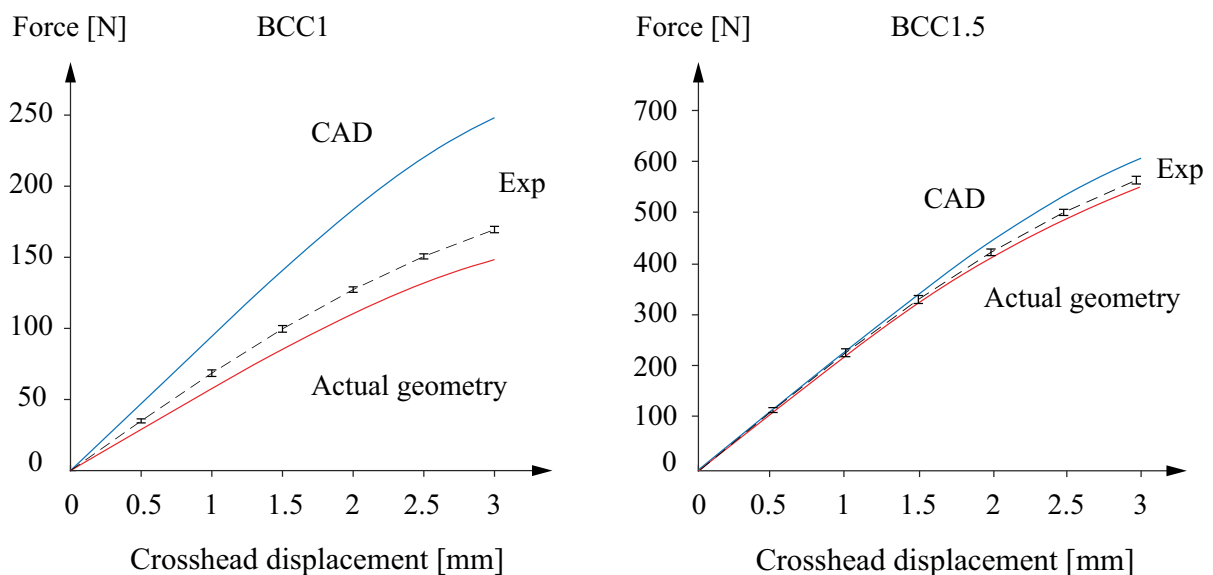


Fig. 8 FEA—experimental force–displacement plots comparison of BCC1 (left) and BCC1.5 (right) specimens. The blue lines represent the numerical results obtained from the CAD nominal model, while the red lines the actual geometry reconstruction

geometrical deviation, but their section was still circular. However, the diameter of those struts was about 25% smaller than the nominal CAD for the BCC and between 10 and 15% for BCC1.5 (Table 2).

Using the corrected geometry allowed a significant reduction of the deviation between the experimental and numerical force–displacement curves. Compared to previous results, the resulting deviation was negative and equal to 12.5% for BCC1 and 2% for BCC1.5.

Therefore, the residual deviation can be attributed to the material model, which was extracted from bulk specimens and could be microstructurally different from the material composing the thin struts. To corroborate this hypothesis, the presence of internal defects was investigated via a CT scan, as reported in Fig. 9. In contrast with the bulk sample, for the lattice specimen, the presence of internal clustered pores, with a large equivalent diameter can be observed (red dots in Fig. 9). However, the analysis showed that, within the gauge length, the material density of the BCC1 and BCC1.5 is higher (97.8% and 98.1%, respectively) compared to the bulky specimen (96.6%).

This difference in porosity content could explain the negative deviation between the lattice experimental and numerical results, for which the material model has been extracted from the bulk tensile tests. In this case, since the simulation accounted only for the first elastic–plastic field, the major contribution to the material resistance is originated by the overall material resistance which is affected by the distributed pores present in the bulk sample. Conceivably, the clustered pores present in the lattice structures contribute to the final material failure and need to be considered in the case of plastic or failure analysis.

According to Ref. [4], the discrepancy between the amounts of porosity in parts processed by L-PBF/P is related to the ratio between the inner exposed area (hatching) and its perimeter (contour). The higher the ratio is, the higher the amount of porosities is. In the case of thin lattice struts, this ratio tends to be relatively small because the inner section of the struts is relatively negligible. In the bulk section, the inner zones to be exposed are significant.

The obtained result implies that the material behaviour of small features and their mechanical responses differ significantly from bulk samples and

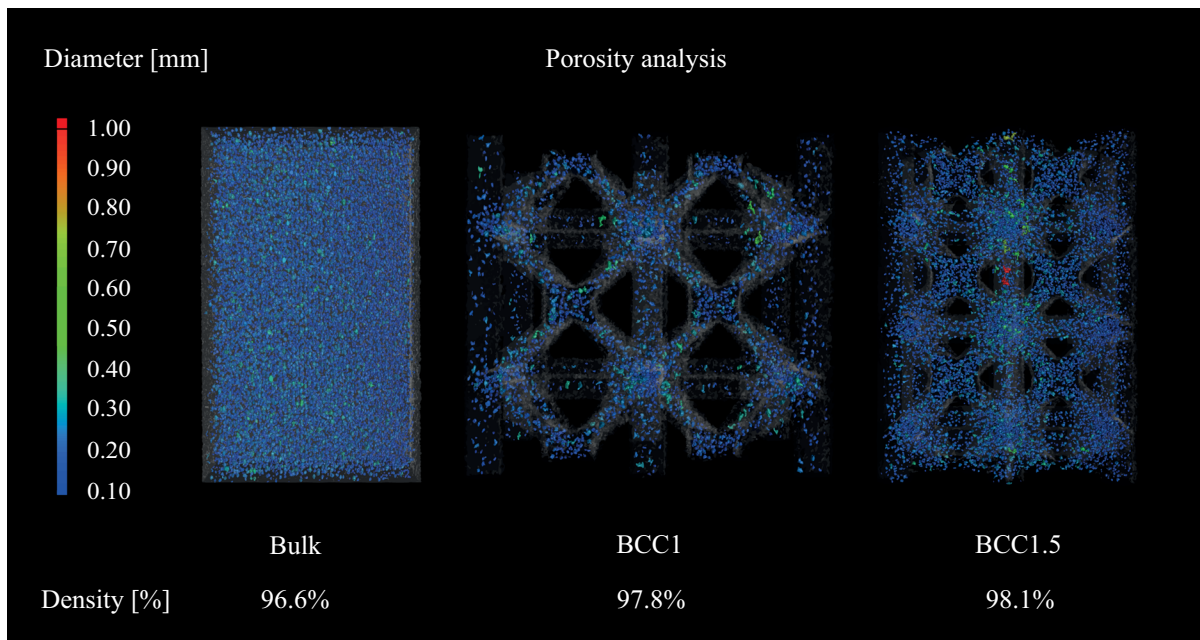


Fig. 9 Porosity analysis results on the bulk, BCC1 and BCC1.5 samples CT-scan reconstructions reported in terms of equivalent diameters comparison where the equivalent diame-

ter is defined as the diameter of a sphere whose volume equals the volume of the pore

require detailed modelling that accounts for local deformation mechanisms.

4 Conclusions

The design of tensile specimens made by lattice structures for mechanical characterisation is complex because it is necessary to assess many elements, including the homogeneity of the stresses during the load and the effect of process-induced defects. This study used a non-linear FEA to evaluate the effectiveness of a new specimen design for reticular lattice in guaranteeing homogeneity of the stress distribution in the load introduction region during the tensile test. The novel geometry used for the test was created following the ISO 527 standard for tensile characterisation. For validation purposes, specimens were manufactured with two strut sizes in PA12 via PBF-LB/P, analysed using a CT scan and tested under a tensile load. The full range of strains was gathered during the test using a DIC analysis.

As forecasted by the FEA, the DIC analysis confirmed the higher strain regions within the gauge length and the forecasted failure locations on a single cell row level in agreement with the experimental failures, validating the numerical analysis. Remarkably, the predicted most stressed regions at a single cell level were in the struts oriented longitudinally to the load axis, where the initial failure was observed experimentally.

CT-Scan analysis displayed a discrepancy between the nominal CAD and manufactured geometry in both the considered strut sizes. This finding explained the observed numerical reaction loads, which were overestimated by 47% and 7% for BCC1 and BCC1.5, respectively, at a 3 mm crosshead displacement. The inferior experimental mechanical responses compared to the results of the numerical analysis performed on the CAD nominal geometry were explained by the ovalisation of the XY struts and the smaller diagonal and z-oriented strut diameters. When the model geometry was compensated for the process-related dimensional deviations, the predictive capability of the numerical analysis improved significantly.

The numerical results deviated marginally from their experimental counterparts. The residual discrepancy may be attributed to the fact that the bulk-derived material model is suboptimal for representing

the thin features of lattice structures since the struts exhibited higher densities than the bulk material. A detailed experimental campaign should be performed to isolate the behaviour of the single struts to establish the correlation between the processed material for thin features and the corresponding mechanical behaviour.

Author contributions Conceptualisation, Methodology, Formal analysis, and investigation: Danilo Bruson and Manuela Galati; Visualisation and Writing—original draft: Danilo Bruson; Writing—review and editing: Manuela Galati and Luca Iuliano; Resources: Luca Iuliano; Supervision: Manuela Galati.

Funding Open access funding provided by Politecnico di Torino within the CRUI-CARE Agreement.

Availability of data and materials The authors declare that the data supporting the findings of this study are available within the paper.

Declarations

Conflict of interest The authors declare that they have no conflict of interest.

Ethical approval Not applicable.

Open Access This article is licensed under a Creative Commons Attribution 4.0 International License, which permits use, sharing, adaptation, distribution and reproduction in any medium or format, as long as you give appropriate credit to the original author(s) and the source, provide a link to the Creative Commons licence, and indicate if changes were made. The images or other third party material in this article are included in the article's Creative Commons licence, unless indicated otherwise in a credit line to the material. If material is not included in the article's Creative Commons licence and your intended use is not permitted by statutory regulation or exceeds the permitted use, you will need to obtain permission directly from the copyright holder. To view a copy of this licence, visit <http://creativecommons.org/licenses/by/4.0/>.

References

1. Murchio S, Dallago M, Zanini F, Carmignato S, Zappini G, Berto F, Benedetti M (2021) Additively manufactured Ti–6Al–4V thin struts via laser powder bed fusion: effect of building orientation on geometrical accuracy and mechanical properties. *J Mech Behav Biomed Mater*. <https://doi.org/10.1016/j.jmbbm.2021.104495>
2. Sombatmai A, Uthaisangsuk V, Wongwises S, Promopatum P (2021) Multiscale investigation of the influence of geometrical imperfections, porosity, and size-dependent features on mechanical behavior of additively

- manufactured Ti-6Al-4V lattice struts. *Mater Des* 209:109985. <https://doi.org/10.1016/J.MATDES.2021.109985>
3. Hossain U, Ghouse S, Nai K, Jeffers JRT (2021) Mechanical and morphological properties of additively manufactured SS316L and Ti6Al4V micro-struts as a function of build angle. *Addit Manuf* 46:102050. <https://doi.org/10.1016/J.ADDMA.2021.102050>
 4. Pavan M, Craeghs T, Verhelst R, Ducatteuw O, Kruth JP, Dewulf W (2016) CT-based quality control of laser sintering of polymers. *Case Stud Nondestruct Test Eval*. <https://doi.org/10.1016/j.csndt.2016.04.004>
 5. Neff C, Hopkinson N, Crane NB (2020) Selective laser sintering of diamond lattice structures: experimental results and FEA model comparison. In: *Proceedings—26th annual international solid freeform fabrication symposium—an additive manufacturing conference*, SFF 2015
 6. Gümüş S, Lackner JM, Polat Ş, Kraschitzer W, Hanning H, Bayram A, Alkan A (2018) Failure behavior of PA12 based SLS lattice structure with macro-porosity. In: *MATEC web of conferences*. <https://doi.org/10.1051/mateconf/201818803007>
 7. Prithvirajan R, Balakumar C, Arumaikkannu G (2019) Effect of strut diameter on compressive behaviour of selective laser sintered polyamide rhombic dodecahedron lattice. In *Materials today: proceedings*. <https://doi.org/10.1016/j.matpr.2020.09.684>
 8. Bai L, Gong C, Chen X, Sun Y, Xin L, Pu H, Luo J (2020) Mechanical properties and energy absorption capabilities of functionally graded lattice structures: experiments and simulations. *Int J Mech Sci*. <https://doi.org/10.1016/j.ijmecsci.2020.105735>
 9. Gorny B, Niendorf T, Lackmann J, Thoene M, Troester T, Maier HJ (2011) In situ characterization of the deformation and failure behavior of non-stochastic porous structures processed by selective laser melting. *Mater Sci Eng A* 528(27):7962–7967. <https://doi.org/10.1016/J.MSEA.2011.07.026>
 10. Yan C, Hao L, Hussein A, Raymont D (2012) Evaluations of cellular lattice structures manufactured using selective laser melting. *Int J Mach Tools Manuf* 62:32–38. <https://doi.org/10.1016/J.IJMACHTOOLS.2012.06.002>
 11. Gümürük R, Mines RAW (2013) Compressive behaviour of stainless steel micro-lattice structures. *Int J Mech Sci* 68:125–139. <https://doi.org/10.1016/J.IJMECS.2013.01.006>
 12. Ahmadi SM, Yavari SA, Wauthle R, Poursan B, Schrooten J, Weinans H, Zadpoor AA (2015) Additively manufactured open-cell porous biomaterials made from six different space-filling unit cells: the mechanical and morphological properties. *Materials*. <https://doi.org/10.3390/ma8041871>
 13. Leary M, Mazur M, Elambasseril J, McMillan M, Chirent T, Sun Y, Brandt M (2016) Selective laser melting (SLM) of AlSi12Mg lattice structures. *Mater Des* 98:344–357. <https://doi.org/10.1016/J.MATDES.2016.02.127>
 14. Leary M, Mazur M, Williams H, Yang E, Alghamdi A, Lozanovski B, Brandt M (2018) Inconel 625 lattice structures manufactured by selective laser melting (SLM): mechanical properties, deformation and failure modes. *Mater Des* 157:179–199. <https://doi.org/10.1016/J.MATDES.2018.06.010>
 15. Drücker S, Inman S, Fiedler B (2020) Simulation and optimization of the load introduction geometry of additively manufactured lattice structure specimens. In: *ECCM 2018—18th European conference on composite materials*
 16. Maconachie T, Leary M, Lozanovski B, Zhang X, Qian M, Faruque O, Brandt M (2019) SLM lattice structures: properties, performance, applications and challenges. *Mater Des* 183:108137. <https://doi.org/10.1016/J.MATDES.2019.108137>
 17. Alsalla H, Hao L, Smith C (2016) Fracture toughness and tensile strength of 316L stainless steel cellular lattice structures manufactured using the selective laser melting technique. *Mater Sci Eng A*. <https://doi.org/10.1016/j.msea.2016.05.075>
 18. Liu W, Li Y, Liu B, Wang G (2020) Development of a novel rectangular–circular grid filling pattern of fused deposition modeling in cellular lattice structures. *Int J Adv Manuf Technol*. <https://doi.org/10.1007/s00170-020-05461-0>
 19. Jung J, Meyer G, Greiner M, Mittelstedt C (2023) Load introduction specimen design for the mechanical characterisation of lattice structures under tensile loading. *J Manuf Mater Process*. <https://doi.org/10.3390/jmmp7010037>
 20. Drücker S, Schulze M, Ipsen H, Bandegani L, Hoch H, Kluge M, Fiedler B (2021) Experimental and numerical mechanical characterization of additively manufactured Ti6Al4V lattice structures considering progressive damage. *Int J Mech Sci*. <https://doi.org/10.1016/j.ijmecsci.2020.105986>
 21. Porter DA, Di Prima MA, Badhe Y, Parikh AR (2022) Nylon lattice design parameter effects on additively manufactured structural performance. *J Mech Behav Biomed Mater*. <https://doi.org/10.1016/j.jmbbm.2021.104869>
 22. Viccica M, Galati M, Calignano F, Iuliano L (2022) Design, additive manufacturing, and characterisation of a three-dimensional cross-based fractal structure for shock absorption. *Thin-Walled Struct* 181:110106. <https://doi.org/10.1016/J.TWS.2022.110106>
 23. Drücker S, Lüdeker JK, Blecken M, Kurt A, Betz K, Kriegesmann B, Fiedler B (2022) Probabilistic analysis of additively manufactured polymer lattice structures. *Mater Des* 213:110300. <https://doi.org/10.1016/J.MATDES.2021.110300>
 24. Vanderesse N, Richter A, Nuño N, Bocher P (2018) Measurement of deformation heterogeneities in additive manufactured lattice materials by digital image correlation: strain maps analysis and reliability assessment. *J Mech Behav Biomed Mater*. <https://doi.org/10.1016/j.jmbbm.2018.07.010>
 25. Huynh L, Rotella J, Sangid MD (2016) Fatigue behavior of IN718 microtrusses produced via additive manufacturing. *Mater Des*. <https://doi.org/10.1016/j.matdes.2016.05.032>
 26. BS-EN-ISO-527-2 (2012) BS EN ISO 527-2 plastics—determination of tensile properties, Part 2: test conditions for moulding and extrusion plastics. Part, 1

27. Maskery I, Aremu AO, Simonelli M, Tuck C, Wildman RD, Ashcroft IA, Hague RJM (2015) Mechanical properties of Ti-6Al-4V selectively laser melted parts with body-centred-cubic lattices of varying cell size. *Exp Mech*. <https://doi.org/10.1007/s11340-015-0021-5>
28. McKown S, Shen Y, Brookes WK, Sutcliffe CJ, Cantwell WJ, Langdon GS, Theobald MD (2008) The quasi-static and blast loading response of lattice structures. *Int J Impact Eng* 35(8):795–810. <https://doi.org/10.1016/j.IJIMPENG.2007.10.005>
29. Lei H, Li C, Meng J, Zhou H, Liu Y, Zhang X, Fang D (2019) Evaluation of compressive properties of SLM-fabricated multi-layer lattice structures by experimental test and μ -CT-based finite element analysis. *Mater Des* 169:107685. <https://doi.org/10.1016/J.MATDES.2019.107685>
30. Mazur M, Leary M, McMillan M, Sun S, Shidid D, Brandt M (2017) Mechanical properties of Ti6Al4V and AlSi12Mg lattice structures manufactured by selective laser melting (SLM). *Laser Addit Manuf Mater Des Technol Appl*. <https://doi.org/10.1016/B978-0-08-100433-3.00005-1>
31. Stoia DI, Linul E, Marsavina L (2019) Influence of manufacturing parameters on mechanical properties of porous materials by selective laser sintering. *Materials*. <https://doi.org/10.3390/ma12060871>
32. Calignano F, Giuffrida F, Galati M (2021) Effect of the build orientation on the mechanical performance of polymeric parts produced by multi jet fusion and selective laser sintering. *J Manuf Process*. <https://doi.org/10.1016/j.jmapro.2021.03.018>
33. British Standards Institute. (1999). ISO 527-1 Plastics—determination of tensile properties—part 1: general principles. ISO standard

Publisher's Note Springer Nature remains neutral with regard to jurisdictional claims in published maps and institutional affiliations.